CellPress
PARTNER JOURNAL

Molecular Plant
Research Article

A Versatile Phenotyping System and Analytics Platform Reveals Diverse Temporal Responses to Water Availability in *Setaria*

Noah Fahlgren[1,3], Maximilian Feldman[1,3], Malia A. Gehan[1,3], Melinda S. Wilson[1], Christine Shyu[1], Douglas W. Bryant[1], Steven T. Hill[1], Colton J. McEntee[1], Sankalpi N. Warnasooriya[1], Indrajit Kumar[1], Tracy Ficor[1], Stephanie Turnipseed[1], Kerrigan B. Gilbert[1], Thomas P. Brutnell[1], James C. Carrington[1], Todd C. Mockler[1] and Ivan Baxter[2,*]

[1]Donald Danforth Plant Science Center, St. Louis, MO 63132, USA

[2]USDA-ARS, Donald Danforth Plant Science Center, St. Louis, MO 63132, USA

[3]These authors contributed equally to this article.

***Correspondence: Ivan Baxter (ivan.baxter@ars.usda.gov)**

http://dx.doi.org/10.1016/j.molp.2015.06.005

ABSTRACT

Phenotyping has become the rate-limiting step in using large-scale genomic data to understand and improve agricultural crops. Here, the Bellwether Phenotyping Platform for controlled-environment plant growth and automated multimodal phenotyping is described. The system has capacity for 1140 plants, which pass daily through stations to record fluorescence, near-infrared, and visible images. Plant Computer Vision (PlantCV) was developed as open-source, hardware platform-independent software for quantitative image analysis. In a 4-week experiment, wild *Setaria viridis* and domesticated *Setaria italica* had fundamentally different temporal responses to water availability. While both lines produced similar levels of biomass under limited water conditions, *Setaria viridis* maintained the same water-use efficiency under water replete conditions, while *Setaria italica* shifted to less efficient growth. Overall, the Bellwether Phenotyping Platform and PlantCV software detected significant effects of genotype and environment on height, biomass, water-use efficiency, color, plant architecture, and tissue water status traits. All ~79 000 images acquired during the course of the experiment are publicly available.

Key words: abiotic/environmental stress, water relations, bioinformatics, development, phenotyping

Fahlgren N., Feldman M., Gehan M.A., Wilson M.S., Shyu C., Bryant D.W., Hill S.T., McEntee C.J., Warnasooriya S.N., Kumar I., Ficor T., Turnipseed S., Gilbert K.B., Brutnell T.P., Carrington J.C., Mockler T.C., and Baxter I. (2015). A Versatile Phenotyping System and Analytics Platform Reveals Diverse Temporal Responses to Water Availability in *Setaria*. Mol. Plant. **8**, 1520–1535.

INTRODUCTION

With growing and more affluent worldwide populations, agricultural crop yields will need to increase significantly by 2050 (Ray et al., 2013; Gerland et al., 2014). Sustainably increasing crop yields in the face of changing environments (IPCC, 2014), and doing so with a smaller environmental footprint, is one of the most pressing global challenges of the 21st century. With changing climate, more prevalent episodes of regional drought and damage due to precipitation extremes will limit agricultural productivity (IPCC, 2014). Salination of agricultural lands and low soil fertility are also increasingly important limitations to crop productivity in many regions.

Advances in DNA sequencing technology have facilitated rapid progress in plant genomics, which has accelerated traditional breeding, molecular marker-assisted breeding, genome editing, and other approaches for crop improvement. Application of genomic technologies, however, is limited by the ability to reliably quantify plant traits (phenotypes). Traits can range in scale from gene expression to yield in the field. Variation in most traits is quantitative, with contributions from multiple genetic loci. Use of genetically defined populations, such as recombinant inbred

Published by the Molecular Plant Shanghai Editorial Office in association with Cell Press, an imprint of Elsevier Inc., on behalf of CSPB and IPPE, SIBS, CAS.

lines (RILs), near-isogenic lines, or accession/association panels, can be used to identify the underlying genetic bases for phenotypes, but only when subtle changes in phenotype are accurately and consistently quantified (Benfey and Mitchell-Olds, 2008). Consequently, plant phenotyping is widely regarded as the rate-limiting step in crop improvement using genome-enabled approaches (Furbank and Tester, 2011; McCouch et al., 2013).

Abiotic stresses can have variable or gradual effects that depend on plant developmental stage. Therefore, measuring phenotypes over time is necessary for in-depth understanding of plant stress responses (Richards and Thurling, 1978; Schoffl, 1998; Mahfoozi, 2001). Destructive methods of assessing plant phenotypes have been used in the majority of studies (Furbank and Tester, 2011), but such methods do not allow traits of discrete individuals to be compared over time. Accordingly, destructive sampling requires an exponential increase in sampling population size with each time point added. Non-invasive and non-destructive techniques permit temporal examination of traits in individual plants, reducing the number of plants needed and permitting larger populations to be examined. The emerging field of plant phenomics, the high-throughput, non-destructive examination of plant growth and development in field or controlled-environment settings, provides new technologies that increase the accuracy and speed of data collection and analysis (Furbank and Tester, 2011). Current non-destructive phenomics technologies focus on a number of traits that, directly or indirectly, reflect chlorophyll content, carotenoid content, photosynthesis, transpiration, plant water content, biomass, and height (White et al., 2012; Andrade-Sanchez et al., 2014).

Phenotyping in the field has all the advantages and disadvantages associated with field-based research. For example, field phenomics allows crop-sized plants to be examined in a natural environmental setting, but field-grown plants are subject to discrete seasonal growing periods and uncontrollable environmental conditions that increase experimental variability. Although a less natural setting, controlled-environment phenomics platforms (Hartmann et al., 2011; Klukas et al., 2014) allow (1) precise control of environmental variables and treatments, (2) experimental replication under reproducible conditions, and (3) better control of instrument placement and functionality. Controlled-environment phenotyping also enables faster experimental turnover, which expedites the cyclical development of image processing algorithms and proxy measurement models that are applicable to both field and controlled-environment phenomics.

The Bellwether Phenotyping Platform combines automated, controlled-environment plant growth with high-throughput, non-destructive imaging and is representative of the next wave of phenotyping platforms aimed at relieving bottlenecks of phenomics data collection. Following data collection, image processing and trait analysis are the next barrier to understanding the underlying biology in high-throughput phenotyping data. Standardized methods for processing image-based, high-throughput plant phenomics data lag behind high-throughput sequencing analysis tools in part because of the variety of commercial and non-commercial platforms used, the numerous research focus areas, and the variety of species and treatments. There is a growing plant phenomics community (http://www.plant-phenotyping.org/) and an excellent database of both commercial and open-source plant image processing software (http://www.plant-image-analysis.org/; Lobet et al., 2013). However, we chose to develop a new trait extraction software platform for daily high-throughput image analysis, Plant Computer Vision (PlantCV). PlantCV is written in a scripting language that has been shown to be accessible to biologists (Mangalam, 2002; Dudley and Butte, 2009), is compatible with a variety of image types and sources, and has a community contribution schema that has been successful for other bioinformatics resources (Oliphant, 2007; Hunter, 2007).

The utility of the system and software is demonstrated here using *Setaria* species and RILs grown under different water conditions. The C4 model monocot *Setaria viridis* (green millet) and the drought-tolerant domesticated crop *Setaria italica* (foxtail millet) (Zhang et al., 2007; Lata et al., 2010, 2011) are closely related to each other and to important crops with similar architecture, such as maize, sorghum, miscanthus, and switchgrass (Brutnell et al., 2010; Li and Brutnell, 2011; Sage and Zhu, 2011). Given the relatively limited understanding of monocot stress responses compared with *Arabidopsis* (Bray, 1997; Wilkins et al., 2010), and the importance of cereal crops as sources of food (Ray et al., 2013), *Setaria* has emerged as a useful model system to explore fundamental aspects of monocot biology (Nelson and Dengler, 1997; Kellogg, 1999; Doust, 2007a; Jia et al., 2013; Qie et al., 2014). Concerted data collection with the Bellwether Phenotyping Platform and analysis with PlantCV detected fundamentally different temporal responses to water availability between the wild and domesticated *Setaria* species. The wild *Setaria* line maintains water-use efficient growth while the domesticated line shifts to less water-use efficient growth in water sufficiency. This publicly available *Setaria* dataset of ~79 000 images, which is available on the iPlant Data Store (Goff et al., 2011) and through the Bio-Image Semantic Query User Environment (BisQue) platform (Kvilekval et al., 2010; also see http://plantcv.danforthcenter.org/pages/data.html), represents the next generation of big data to query for phenotypes that affect important yield traits.

RESULTS AND DISCUSSION

Design of the Bellwether Phenotyping Platform

The design of the platform was key to the execution of the *Setaria* water-limitation experiment described below. The system comprises a Conviron (Winnipeg, Canada) climate-controlled growth house integrated with a multi-camera digital imaging system (LemnaTec Scanalyzer$^{3D\text{-}HT}$, Figure 1A). This automated high-throughput platform allows for repeated non-destructive image capture for multi-parametric analysis and provides valuable information on the physiological changes of the plants over time. The integration of Conviron and LemnaTec technologies and other custom design decisions was motivated by the goal of tightly controlling the environment while analyzing large numbers of plants. In comparison with greenhouse environments where external factors such as cloud cover or extreme seasonal temperatures can greatly affect the environmental conditions and introduce unpredictable variables into an experiment, the control of this system facilitates reproducible temporal phenotyping of plants.

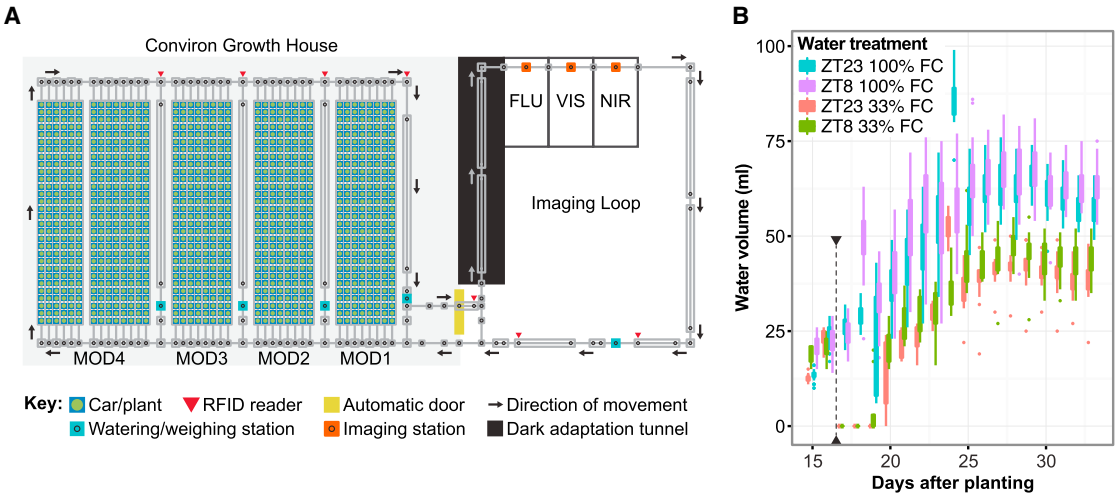

Figure 1. Bellwether Phenotyping Platform at the Donald Danforth Plant Science Center.

(A) Diagram of the platform.

(B) The volume of water added to *S. viridis* plants during morning (ZT23) and evening (ZT8) water applications. The arrowheads indicate the day that the 33% FC water treatment started.

A compact network of over 180 m of conveyor belts is used to store and transport 1140 plants in pots 10 cm (4 inches) in diameter to and from watering and imaging stations inside the chamber. The conveyor belts are divided into four distinct modules (MOD1–4), which can be controlled independently or as a whole, providing flexibility in experimental design (Figure 1A). A custom-engineered automated door maintains the growth house environment while providing a route for plants to leave and enter the chamber (Figure 1A). The pots are moved in radiofrequency identification (RFID) chipped carriers, which are associated with plant barcodes that are used to organize collected image data and metadata, including water treatment instructions. Each MOD contains a precision dual-tank watering station that is equipped with a scale, which can be configured to water to a fixed volume or to a target weight, which makes a variety of experimental watering schemes possible including periodic water stress. When watered to an experimentally determined target weight, the real-time weight of each pot is used to calculate the amount of water required to reach the predetermined target.

The decision to install four watering stations inside the growth house (Figure 1A) allows for tight control of soil water status while maintaining imaging throughput. Due to the single-file movement of the carriers through the closed-loop conveyor system, a single watering station would have limited the number of water applications possible in a day and would have competed with imaging time. A single watering station would have also introduced a significant temporal divide between the first and last watered plants, adding variability into the treatment groups and confounding water usage analysis. Instead, four plants can be watered simultaneously, improving efficiency and drastically reducing the time required to water the entire population (less than 2 h).

The digital imaging loop connected to the growth house consists of a dark adaptation tunnel and three distinct imaging chambers: visible light (VIS), photosystem II (PSII) fluorescence, and near-infrared (NIR) (Figure 1A). The imaging stations are described in detail in the sections below. Visible light imaging is used to capture and quantify morphological parameters such as plant shape, color, size, and biomass. PSII fluorescence is used for the analysis of photosynthetic efficiency, which can be used to estimate the response to plant treatment or stress, or to measure photosynthetic differences among genetically diverse lines (Maxwell and Johnson, 2000; Garg et al., 2002; Fernández-García et al., 2014; Talukder et al., 2014). NIR imaging is used to estimate the tissue water content (Carter, 1991; Peñuelas and Filella, 1998; Seelig et al., 2008, 2009). The throughput of the system depends on experimental design, the desired number of output images, the frequency of water treatment, and is limited by the transport rate of the conveyor. At full capacity (1140 plants), using all imaging chambers to capture top-view and four side-view images (PSII top-view only), the entire population can be imaged in approximately 30 h, typically yielding between 25 000 and 37 500 images per week.

Setaria Water-Limitation Experiment

With target-weight water treatments possible on the Bellwether Platform, the water available to the plant should be tightly controlled. To increase the precision of target-weight watering, pre-filled pots of soil were used. The use of pre-filled pots also helped to ensure that soil density was similar between pots. To test the platform and examine the response of *Setaria* to water-limited conditions, 10 *Setaria* lines were grown under four different water regimes (full-water capacity: 100% FC, 66% FC, 33% FC, and 0% FC) imposed 17 days after planting (DAP) and maintained for 17 days. Plants were watered twice a day starting at ZT8 (Zeitgeber Time) and ZT23. For more experimental details see Materials and Methods. The lines used were *S. viridis* (accession A10), *S. italica* (accession B100), and eight randomly selected RILs derived from a cross of *S. viridis* × *S. italica* (Devos et al., 1998; Wang et al., 1998; Bennetzen et al., 2012). An average of 15 plants per line per water treatment

were loaded onto the system. Additional *S. viridis* and *S. italica* plants were also loaded for parallel destructive physiological tests.

The plants that received no water after 17 DAP died within 7 days of treatment and were removed from the system leaving 33% FC as the severest water-deficit treatment. Comparisons between 33% and 100% FC were the focus of subsequent analysis. Figure 1B shows the volume of water added at each treatment time point for *S. viridis* plants watered to 100% and 33% FC. The differences between the two water treatment set points can be seen clearly after the 33% pots complete their dry down from full water 17–19 DAP. As the plants grow and transpire, more water is needed to return the pots to their set points. More water was added compared with the days surrounding 18 DAP when the second water application was delayed and 24 DAP when the target-weight point was raised to account for increasing biomass of the plants (Figure 1B).

Setaria Image Acquisition

During the experiment, *Setaria* plants varied in height from 0.9 cm to 54.5 cm, so a scaled field of view (adjusted optical zoom level) was used during image acquisition to maximize the image pixels (px) dedicated to plant material, and not background space. Consequently, plant traits measured in pixels from images taken at different zoom levels are not directly comparable because of the difference in the field of view. A reference object with known dimensions was imaged using the VIS side-view and top-view cameras at different zoom levels. To compare digital traits across zoom levels, scaling factors were calculated for both area and length traits using zoom-scaling functions (see Supplemental Experimental Procedures).

PhenoFront Database Access Tool

Image and water volume data from LemnaTec phenotyping systems are stored in a PostgreSQL database, but images themselves are stored separately in raw format. To provide distributed access to image and water treatment data, an independent database interface tool (PhenoFront) was developed. It was necessary to develop a new database access tool rather than use existing open-source interface tools (Klukas et al., 2014) because the image storage structure of the LemnaTec version 4.0 database changed significantly from previous versions.

PhenoFront has a convenient web-based user interface to the phenotyping database and provides an experiment query-building tool that allows users to extract specific image and water treatment data. Importantly, PhenoFront was built with diverse image types in mind (e.g. color vs grayscale; 8-bit vs 16-bit) and allows access to images without conversion to a single file format. Queries can be directly downloaded to the user's computer, or data can be downloaded to a remote server capable of high-throughput image processing using utilities such as Wget (http://www.gnu.org/software/wget/wget.html) or cURL (http://curl.haxx.se/). PhenoFront is available at https://github.com/danforthcenter/PhenoFront.

Datasets extracted with PhenoFront are structured by data acquisition events (snapshot: weighing/watering, imaging) and a single metadata text file contains the experimental and system parameters associated with each event. Image metadata from the experiment presented here include experiment identification code; snapshot folder identification number; alphanumeric barcode encoded with species identification, line identification, water treatment group, and unique plant number; unique snapshot timestamp; weight and water volume information; individual image file names included in the snapshot directory. The structured datasets can be easily read by analysis software and are convenient for public data sharing.

Although strides have been made to create resources for image processing on the iPlant cyber infrastructure (Kvilekval et al., 2010), a dedicated centralized database for sharing published plant phenotyping image data has not been designated. Although a few plant phenomic datasets are publicly available (Fahlgren et al., 2015), this is the largest publically available dataset of above-ground plant tissue to date (79 200 images of 823 plants). Image data from this experiment are available via http://plantcv.danforthcenter.org/pages/data.html in Portable Network Graphics (PNG) and Joint Photographic Experts Group (JPEG) formats. JPEG format images with lossy compression consume approximately 11-fold less storage size, but comparisons of image datasets in JPEG and PNG format revealed significant differences in some analyzed traits (see Materials and Methods). Establishing a dedicated centralized database that is designed to deposit and access large plant phenomic datasets and standardized metadata is vital for aggregating and curating data for the community. The phenomics community will need to collectively consider formats, data and metadata structure, minimal information standards, ontologies, and other sharing issues. Implementing these phenotyping standards will expedite tool development and alleviate barriers to crop improvement.

Phenotype Extraction Using PlantCV Software

High-throughput plant phenotyping has the potential to improve modeling of genotype by environment interactions and to expedite identification of germplasm that could increase the yield and productivity of crop plants. With numerous commercial and custom-built image-based phenotyping platforms in existence, it is unlikely that standard hardware will be used to capture image-based phenomics data in the near future. Lack of standard hardware thus requires each new platform to go through a significant initialization period and a gambit of validation experiments, many of which are described in this study. Despite different hardware platforms, image analysis and trait extraction are common ground between image-based phenotyping platforms. Therefore, open-source trait extraction software with a mechanism for community development will help to alleviate the phenotyping bottleneck on crop improvement.

Available commercial and open-source plant image processing software range in their capabilities, flexibilities, and underlying programming languages and largely focus on analysis of single cells, leaves, roots, or plants with rosette architecture (http://www.plant-image-analysis.org; Lobet et al., 2013). There are analysis tools in the Plant Image Analysis database, such as LemnaGrid (https://www.lemnatec.com) (Munns and Tester, 2008; Berger et al., 2010; Golzarian et al., 2011; Honsdorf et al., 2014), the ImageJ (Abràmoff et al., 2004) plugin HTPheno (Hartmann et al., 2011), and the Java-based open-source

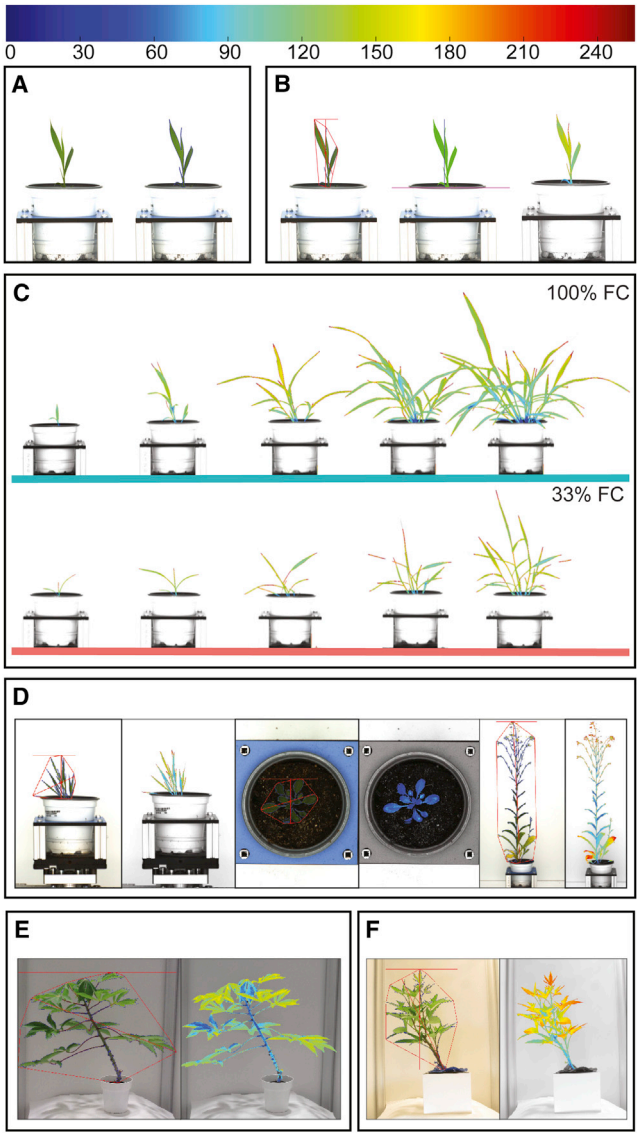

Figure 2. PlantCV Image Analysis Software Developed at the Donald Danforth Plant Science Center.

(A) Automated identification of plant material from background. Plant is identified (blue outline, right) from the original image (left).

(B) Example of traits extracted by PlantCV. Shape characteristics such as convex hull (left), and height (middle) are extracted from visible images. Differences in color can be visualized by pseudocoloring by HSV, LAB, or RGB color channels (right). *S. viridis* is pseudocolored based on the value channel of HSV color space.

(C) PlantCV analysis of traits over time under 100% FC and 33% FC water treatments. Traits such as biomass accumulation, growth rate, and color can be tracked over time under experimental conditions, such as drought, from data collected by PlantCV. *S. viridis* is shown pseudocolored based on the value channel of HSV color space.

(D) Example of PlantCV extracted traits from plant species other than *Setaria*. *Brachypodium distachyon*, *Arabidopsis thaliana*, and *Camelina sativa* are pictured from left to right. Plants are pseudocolored based on the value channel of HSV.

(E) Example of PlantCV analysis of an image of cassava captured by a cell phone camera.

(F) Example of PlantCV analysis of an image of sweet potato captured by a digital camera.

Integrated Analysis Platform (IAP) (Klukas et al., 2014) that are capable of analyzing larger model plants and crops with diverse architectures (Supplemental Table 1). We developed the open-source and open-development PlantCV image analysis platform to emphasize the following features: flexible user-defined analysis workflows; parallelizable image processing for fast throughput; and a scripting language implementation that lowers the barrier to community contributions that extend functionality. It was important to move away from commercial software for greater control and understanding of the image processing and trait extraction algorithms used to process the data, as well as the freedom to expand analyses at will. While some users may prefer graphical user interfaces for software, script-based programs are easier to develop and the precise workflows are detailed directly in the scripts themselves, enabling reproducible research.

Extraction of temporal plant trait data from images occurs in three steps: (1) isolation of plant material from background (Figure 2A); (2) identification of features (traits) from isolated plants (Figure 2B); and (3) analysis of traits across population, treatments, and time (Figure 2C). PlantCV isolates plant material from background, quantifies plant traits, and populates an SQLite (https://www.sqlite.org/) database that is easily queried for further analysis across treatments, genotypes, and time. In debug mode, PlantCV creates annotated intermediate images for each step of image analysis pipelines (e.g. outlining plant perimeter), allowing users to verify that analysis steps are working as intended. Although *Setaria* images from the high-throughput Bellwether Phenotyping Platform are analyzed here, PlantCV has been used to analyze a variety of plant types (Figure 2D–2F) as well as images captured from non-commercial imaging stations (Figure 2E and 2F). For the *Setaria* experiment here, traits such as height, biomass, and plant architecture were manually measured and are highly correlated with traits computationally extracted by PlantCV (Figures 3–5). Image datasets curated with manual measurements are available at http://plantcv.danforthcenter.org/pages/data-sets/2013/setaria_burnin2.html and are a resource for generating further trait measurement algorithms.

PlantCV software is built upon the open-source libraries OpenCV (Bradski, 2000), NumPy (Oliphant, 2007), and MatPlotLib (Hunter, 2007), and contains pipelines built with modular functions that are currently capable of automated analysis of color and grayscale images from VIS, PSII, and NIR cameras. Separate pipelines are used to process images from different camera types due to differences in image size and dimensions, spectral channels (e.g. color versus grayscale), special processing steps (e.g. PSII imaging, see below), and other factors (e.g. lighting). PlantCV was written in the Python programming language with hopes that the greater phenomics community will utilize and extend its functionality. Although Python is not as efficient as compiled languages (e.g. C or Java) in terms of memory usage and speed of execution (Fourment and Gillings, 2008), it is currently more widely used by biologists and is arguably easier to learn (Mangalam, 2002; Dudley and Butte, 2009). On a single processor, PlantCV can process and extract data from 200–350 images per hour, depending on image size, and the modular script-based architecture allows for easy parallelization. At the Danforth Center, PlantCV is typically run on 10 CPUs. PlantCV

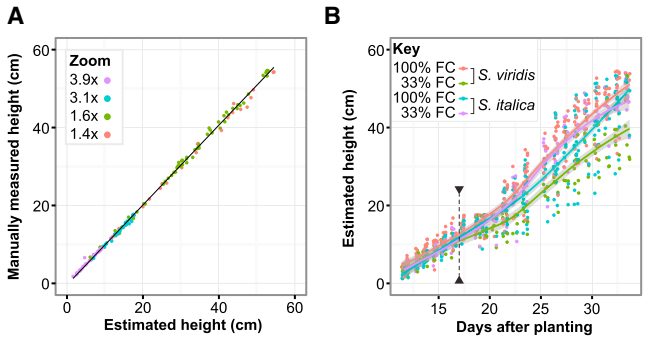

Figure 3. Plant Height Estimated with PlantCV.

(A) Plant height estimated with PlantCV compared with manually measured height. Data shown are for 173 randomly selected VIS side-view images at four different zoom levels. The ordinary least squares linear model with SE is plotted.

(B) Estimated plant height for *S. viridis* and *S. italica* plants from 11 to 33 DAP. Plants watered to 100% or 33% FC are shown. Local regression (LOESS) fitted curves with SE are plotted for each genotype by water treatment group. The arrowheads indicate the day that the 33% FC water treatment started. See also Supplemental Figure 1.

is an open-source resource under a GNU General Public License (GPLv2) share-alike license that can be leveraged for the further development of more complex trait identification modules. PlantCV is also available via GitHub, providing a framework for community contribution that has been successful for other science and Python-based projects such as NumPy (~284 contributors) and MatPlotLib (~294 contributors) (Oliphant, 2007; Hunter, 2007). Community contribution helps to maintain software permanence (Gentleman et al., 2004), which is often a problem for bioinformatics tools maintained by individual laboratories (Gilbert, 2004). PlantCV, PlantCV documentation, tutorials, parallelization scripts, downstream analysis scripts, and a contribution guide can be accessed at http://plantcv.danforthcenter.org.

VIS Image Processing and Traits

The VIS imaging station on the platform captures visible light (400–700 nm) images with two high-resolution (2454 × 2056 pixel) charge-coupled device cameras. One camera is mounted above the plant and the second camera is side-mounted for top- and side-view imaging, respectively. The plant carrier is positioned on a piston lifter with a turner that can rotate the plant 360°. During the *Setaria* experiment, a single top-view and four side-view (0°, 90°, 180°, and 270°) VIS images were acquired per plant per time point. In total, *Setaria* plants were imaged 6399 times from 11–33 DAP for a total of 31 968 VIS images (55 images per plant). The set of images collected for a single plant in one imaging session is defined as a snapshot.

In general, PlantCV VIS image processing pipelines automatically identify background material within the image, such as the carrier, pot, soil, and side paneling. To mitigate plant identification bias due to genotype, developmental age, abiotic treatment, or other experimental parameters, plant material was isolated after several stages of background removal, rather than first thresholding for plant greenness. For a complete description of the VIS image processing steps, please refer to the Supplemental Experimental Procedures and view the PlantCV online documentation.

Plant Height

Plant height was defined as the maximum vertical extent of the plant from the top of the pot. For 173 randomly selected VIS side-view images from all genotypes and treatments, plant height (calibrated using the width of the plant carrier) was manually measured using ImageJ (Abràmoff et al., 2004). For the same image set, plant height was automatically estimated using PlantCV with height scaled to correct for the camera zoom level (see Supplemental Experimental Procedures). Ordinary least squares regression analysis confirmed that PlantCV measured plant height was a good estimator of manually measured height and was robust across changes in camera zoom level (adjusted R^2 = 0.998, slope = 1.02; Figure 3A).

To analyze *Setaria* height more robustly at the population level, estimated plant height was averaged between all four VIS side-view images for each snapshot and the effect of genotype and low water availability on height was calculated. Intrinsic height differences under full-water conditions were observed for the *Setaria* genotypes, particularly from 23 to 33 DAP. *S. viridis* was taller than *S. italica* from 23 to 33 DAP with a mean height ranging from 26.7 to 50.7 cm compared with 22.8 to 49.4 cm, respectively, but the 95% CIs overlapped, suggesting that the difference was marginal at best (Figure 3B). The height of RIL102 was within the range of the two parent lines but the other seven RILs were transgressive; RIL161 was shorter on average than the parents while the others were taller (Supplemental Figure 1). Height for the tallest lines was underestimated because the camera field of view in this experiment was not zoomed out enough to completely capture the tallest plants. For example, truncated plant height due to camera settings is noticeable from 15 to 20 DAP after which the field of view was expanded and plants were fully imaged again (Figure 3B and Supplemental Figure 1). Although thorough surveillance can be used to avoid lapses in coverage due to sub-optimal camera settings, the large number of potentially diverse plants on high-throughput systems makes complete oversight challenging. A better approach would be to add real-time analysis that raises alarm to potential framing issues once preset threshold boundaries are reached. The parallelized rate of PlantCV analysis permits future experiments to implement real-time boundary detection.

In addition to intrinsic height phenotypes, the impact of limited water availability on plant height was also measured. *S. viridis* plants watered to 33% FC starting 17 DAP had a slower vertical growth rate than plants at 100% FC from 21 to 33 DAP (linear change in height = 2.1 and 2.5 cm/day, respectively; Figure 3B). In contrast, *S. italica* plants from 100% and 33% FC groups did not have significantly different vertical growth rates, suggesting that *S. italica* plant height is not tightly coupled to water availability (linear change in height = 2.5 cm/day; Figure 3B). Alternatively, these results could suggest that *S. viridis* responds to extra water availability with more growth while *S. italica* does not. Of the 10 lines analyzed, *S. viridis* has the largest difference in height when comparing the 33% and 100% FC treatment groups (Supplemental Figure 1). The difference in height for the RILs was either similar to *S. italica* or was intermediate between the two parents (Supplemental Figure 1).

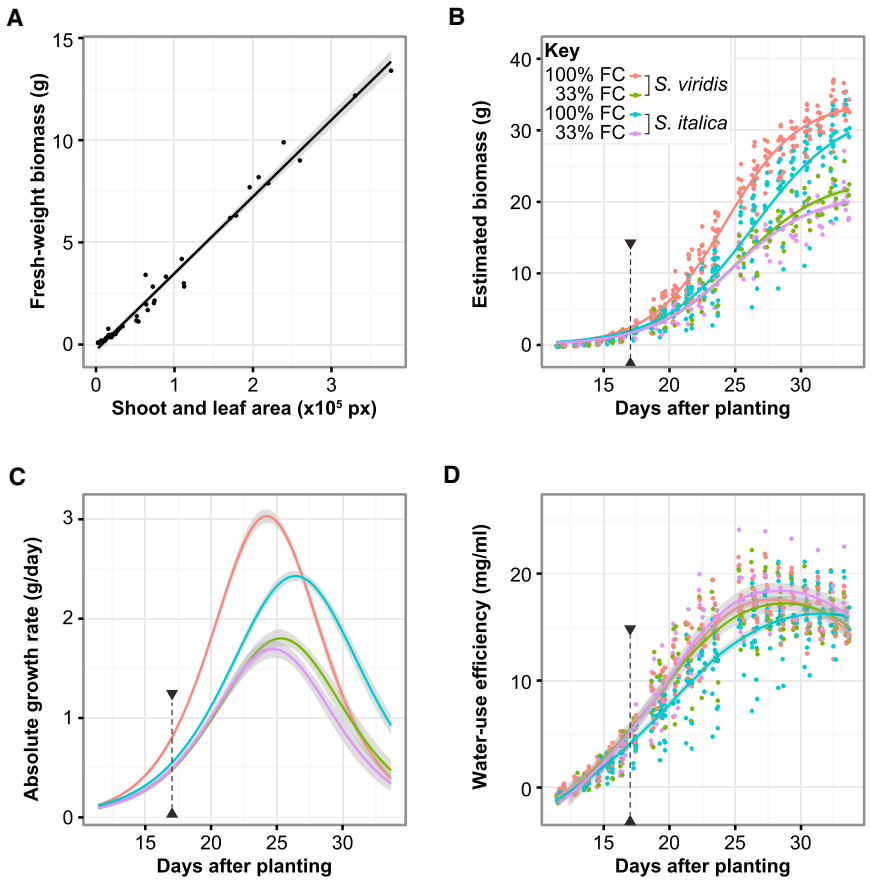

Figure 4. *S. viridis* and *S. italica* Respond Differently to Water-Limited Conditions.
(A) Above-ground fresh-weight biomass modeled using shoot and leaf pixel area from four side-view VIS images. Data shown are for 41 plants for which destructive fresh-weight biomass was measured throughout the experiment. The ordinary least squares linear model with SE is plotted. **(B–D)** Data shown are for *S. viridis* and *S. italica* imaged from 11 to 33 DAP. Plants watered to 100% or 33% FC are shown. Arrowheads indicate the day that the 33% FC water treatment started. **(B)** Modeled fresh-weight biomass. Three-component logistic growth curves with 95% CIs are plotted. **(C)** Absolute growth rates over time with 95% CIs. **(D)** Water-use efficiency, accumulated fresh-weight biomass divided by cumulative water added. LOESS fitted curves with SE are plotted. **(C** and **D)** see color key in **(B)**. See also Supplemental Figures 2 and 3.

Above-Ground Biomass

Throughout the experiment, 41 *S. viridis* and *S. italica* plants randomly selected from the full-capacity water group were collected and the above-ground fresh- and dry-weight biomass were recorded. The images acquired immediately prior to collection were analyzed with PlantCV to measure plant traits that could be used to model biomass. Linear modeling was done with three PlantCV measurements: side-view area, the sum of the above-ground plant pixel area from all four side-view VIS images; top-view area, the plant pixel area from the single top-view VIS image; and plant height, as described above. The initial model included side-view area, top-view area, and height, adjusted for zoom level, and all pairwise interaction terms. A stepwise model selection procedure was done using the Akaike's Information Criterion (Bozdogan, 1987), which resulted in the reduced model:

$$M_{fw} = 3.755 \times 10^{-5} A_{sv} - 0.2704$$

where M_{fw} is fresh-weight biomass and A_{sv} is side-view area (adjusted R^2 = 0.983; Figure 4A). Dry-weight biomass was also modeled efficiently with side-view plant pixel area (adjusted R^2 = 0.976; Supplemental Figure 2). It was hypothesized that residual variation in biomass could be explained by plants that were partially out of frame or by genotype. PlantCV records when plants extend to or past the border of each image, and the model including the out-of-frame status of each plant was accepted over the reduced model ($p < 0.01$, F-test) but only slightly improved the model (adjusted R^2 = 0.986). In contrast, genetic background did not improve the model significantly, suggesting that biomass estimation for *S. viridis* and *S. italica* is robust to *Setaria* species differences, at least within the conditions tested.

Growth Rates and Response to Water Availability

Image-based biomass estimates were used to quantify the impact of limited water availability on *Setaria* fresh-weight biomass (Figure 4 and Supplemental Figure 3). Non-linear least squares regression was used to estimate the growth parameters (three-component logistic model) for each group (genotype by treatment) (Figure 4B and 4C) (Paine et al., 2012). Under water deficit, *S. italica* and *S. viridis* grew at similar rates with a maximum absolute growth rate at ~25 DAP of 1.7 (95% CI, 1.61–1.78 g/day) and 1.8 g/day (95% CI, 1.72–1.89), respectively (Figure 4B and 4C). In contrast, under 100% FC treatment, the maximum absolute growth rate of *S. viridis* was 0.6 g/day more than *S. italica* (3.0 and 2.4 g/day, respectively; 95% CIs, 2.96–3.10 and 2.38–2.48 g/day, respectively) and was reached 2 days earlier (24 and 26 DAP, respectively) (Figure 4C). As a result, the impact of water limitation on fresh-weight biomass was larger and observed more quickly in *S. viridis* compared with *S. italica*. *S. viridis* watered to 33% FC starting at 17 DAP accumulated significantly less biomass relative to the control group from 19 DAP until the end of the experiment (95% CI, 0.6–2.4 g; Figure 4B). *S. italica* watered to 33% FC accumulated significantly less biomass relative to the control group at 28 DAP until the end of the experiment (95% CI, 1.8–7.3 g; Figure 4B). Plant growth and response to the environment is a dynamic process and non-destructive phenotyping was key to understanding the differences between *S. viridis* and *S. italica*. For example, although *S. viridis* grows faster and earlier than *S. italica* under 100% FC treatment, biomass at 33 DAP was similar so end-point biomass measurements would have missed the growth differences between *S. viridis* and *S. italica* (Figure 4B and 4C).

Integrated Water-Use Efficiency

The ability to measure and record the volume of water applied to individual plants (Figure 1B) in combination with the estimated

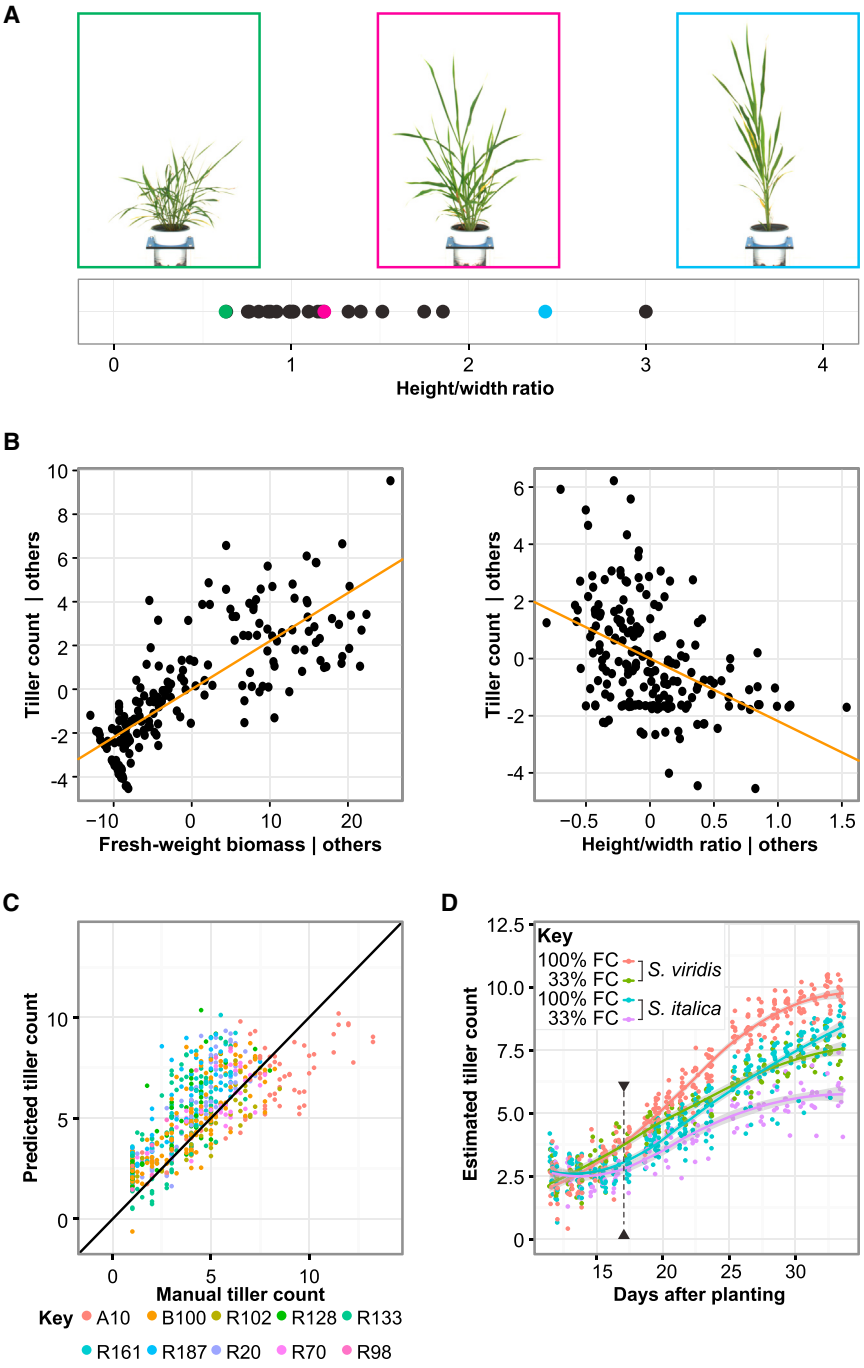

Figure 5. Tiller Count Modeled from Spatial-Independent Morphological Characteristics.

(A) Examples of height/width ratio variation from randomly selected images of plants 25–26 DAP.

(B) Added-variable plots of fresh-weight biomass and height/width ratio from 195 randomly selected images. The ordinary least squares linear model for each partial regression is plotted.

(C) Relationship between manually measured tiller count from 646 randomly selected images and model-predicted tiller count. The line y = x is plotted.

(D) Model-predicted tiller count for *S. viridis* and *S. italica* plants from 11 to 33 DAP. Plants watered to 100% or 33% FC are shown. Arrowheads indicate the day that the 33% FC water treatment started. See also Supplemental Figure 4.

biomass of plants over time (Figure 4B) provides a framework for quantifying plant intrinsic water-use efficiency (WUE). Here intrinsic WUE is operationally defined as the amount of biomass accumulated per milliliter of water applied (units, mg/ml). No significant difference in WUE was observed for *S. viridis* plants watered to 100% or 33% FC ($q > 0.05$; Figure 4D). Therefore, the amount of *S. viridis* accumulated biomass is proportional to the volume of water supplied. In contrast, *S. italica* plants had lower WUE at 100% FC relative to 33% FC, with significant differences observed from 22 to 27 DAP ($q < 0.05$; Figure 4D). This suggests that *S. italica* uses water less efficiently under water-sufficient conditions.

Plant Architecture

The traits discussed above do not require knowledge of specific plant architecture but architectural phenotypes such as tillering and leaf angle can have a significant impact on plant performance (Warnasooriya and Brutnell, 2014). Known differences in plant architecture between the wild *S. viridis* and domesticated *S. italica* include the number of axillary branches and tiller number (Darmency et al., 1987; Doust and Kellogg, 2006; Doust, 2007b; Doust et al., 2009). Computational 3D reconstruction of plant architecture from 2D images would promote accurate estimates of tiller count but would have a significant impact on imaging throughput because of the increase in images per plant per time point needed to enable 3D reconstruction (Phattaralerphong and Sinoquet, 2005; Paproki et al., 2012). Modeling is an alternative approach that can be used to predict the number of tillers given one or more morphological parameters that are more easily measured.

In a first attempt at generating a predictive model for *Setaria* architecture, tiller number, tiller angle (angle between the two outermost tillers), and leaf angle (angle between the leaf and tiller of the first leaves on the two outermost tillers) values were measured using ImageJ (Abràmoff et al., 2004) on 58 randomly selected images of plants 25 and 26 DAP. The results were compared with two morphological traits that are simple to calculate using PlantCV: height/width ratio (HW, height divided by extent-x; Figure 5A) and solidity (plant area divided by convex hull area). HW was significantly correlated ($p < 0.01$) with all three manually measured traits but the best model for HW, which accounted for 37% of the variance in an ANOVA analysis, included only tiller angle and leaf angle (see Materials and Methods). Solidity was not significantly correlated with any of the manually measured traits. While the HW ratio is not

inherently a measure of a single plant architecture trait, it can serve as an easily obtainable proxy for further analysis. To generate a predictive model for tiller count, HW and several other traits were examined. Tillers were manually counted for 195 randomly selected images. HW, solidity, fresh-weight biomass, width (extent-x), and height were tested as potential explanatory variables for manual tiller counts. Ordinary least squares regression was used to generate a model for the number of tillers:

$$TC = 0.220M_{fw} - 2.19HW + 5.26$$

where TC is the number of tillers, M_{fw} is fresh-weight biomass, and HW is the height/width ratio. The tiller model explained 64% of the variation in tiller number (Figure 5B). To further test the tiller model, tillers were counted for a second set of 646 randomly selected images. The accuracy of the tiller model to predict tiller number in the second set of 646 images was assessed and the mean difference between predicted and manual tiller number was 0.92 tillers (95% CI, 0.80–1.04 tillers; Figure 5C). Although there are clearly other variables that contribute to the tiller model, the predicted tiller count model generated with spatial-independent morphological characteristics can serve as a proxy measurement of *Setaria* architecture.

The tiller count model was used to predict tiller numbers in *S. viridis*, *S. italica*, and the eight *S. viridis* × *S. italica* RILs under 100% FC and 33% FC water treatments. For all *Setaria* genotypes, tiller number decreased with reduced-water treatment but the intensity and speed of response varied (Figure 5C and Supplemental Figure 4). The predicted tiller count for *S. viridis* is greater than that for *S. italica* under both 100% FC and 33% FC water conditions (Figure 5D), which is consistent with known architectural differences between the two genotypes (Darmency et al., 1987; Doust and Kellogg, 2006; Doust, 2007b; Doust et al., 2009). Predicted tiller number appears to be an introgressive trait for the RILs analyzed (Supplemental Figure 4) and can be genetically mapped in a larger *S. viridis* × *S. italica* RIL population.

Color Analysis

Color is often used to gauge plant health in response to biotic and abiotic treatment, or to identify lines that have possible defects in pigment development and thus changes in photosynthesis (Albrecht-Borth et al., 2013; Kremnev and Strand, 2014; Kunz et al., 2014; Satou et al., 2014; Neilson et al., 2015). For each identified plant pixel, PlantCV records intensity values of color data for each of the three color channels of RGB (red, green, blue), HSV (hue, saturation, value), and LAB (lightness, green-magenta, blue-yellow) color space, yielding a set of three histograms for each color space. The RGB data are presented here because images are captured in RGB color space. Results from interpolated HSV and LAB color space are included in the Supplemental Information but interpretations of these results concur with the RGB color space (Supplemental Figures 5–8). The VIS images obtained via PhenoFront are 8-bit color images, therefore each pixel in each channel can have a maximum intensity value of 2^8 or 256. PlantCV was used to normalize the *Setaria* color histograms by the number of plant pixels (plant size) and these values are averaged by the four side-view angles.

Color data were evaluated to determine if water treatment effects could be distinguished 25–26 DAP in *S. viridis* where there is a significant difference in biomass under reduced water (Supplemental Figures 5 and 6). Principal component analysis (PCA) visibly separated full-water from reduced-water treatment along PC2, which captures 16% of variation (Supplemental Figures 5 and 6). Spearman correlation analysis found that PC2 was significantly negatively correlated ($p < 0.01$; rho = −0.7056) with water treatment 25–26 DAP in *S. viridis*. Principal component regression found that a two-component model of PC1 and PC2 covers 62% of the variation seen in treatment 25–26 DAP (Supplemental Figures 5 and 6). Therefore, *Setaria* color can be used to distinguish water treatments 25–26 DAP. PCA using all RGB color data as explanatory variables from *S. viridis* 17 and 18 DAP did not visibly separate full water from 33% FC (Supplemental Figures 5 and 6) and a two-component regression model included only 0.45% of the variance explained by treatment. Consequently, *Setaria* color does not appear to be as early an indication of drought as biomass.

Color analysis was able to discriminate plant genotypes before treatment was applied, which was not the case for estimated plant biomass (Supplemental Figure 3). PCA of RGB color data prior to water treatment (11–12 DAP) found that PC1 captures 41% of variation in color and separates RIL161 (Figure 6A) from the other genotypes. The RIL161 line was distinguishable from the other *Setaria* lines and appears to be pale in pigmentation (Figure 6B). The seven other RIL lines (Figure 6A) grouped along PC1 and PC2 with the parent lines, *S. viridis* (Figure 6A, left) and the majority of *S. italica* (Figure 6A, right). Seventeen of 112 *S. italica* plants clustered with RIL161 plants (Figure 6A, right). Investigation of *S. italica* plants that clustered with the RIL161 plants revealed that they are paler in color compared with *S. italica* that group with *S. viridis* and the other RILs (Figure 6B). The color PC1 trait appears to be a transgressively segregating phenotype in RIL161 compared with the majority of parent phenotypes and may be genetically mapped in the larger *S. viridis* × *S. italica* RIL population. The color PC1 trait may also be associated with a photosynthetic trait, since RIL161 plants are not only pale but also shorter on average compared with other lines (Supplemental Figure 1).

PSII Image Traits

For more information on PSII image processing, please refer to the Supplemental Experimental Procedures. Comparison with plant architecture traits from the VIS system revealed that F_v/F_m is strongly correlated with plant height in a Spearman correlation analysis (rho = −0.859, $p < 0.01$; Supplemental Figure 9). To further test if plant height significantly influences F_v/F_m measurements, a 3D-printed staggered platform was designed and built to examine ~4 cm^2 of excised *Nicotiana benthamiana* leaf tissue at fixed heights (Supplemental Figure 9B and 9C). *N. benthamiana* was used because the leaves are large enough for tissue from a single leaf to be used at all four platform levels. PSII analysis of the 3D-printed platform confirmed that height significantly negatively correlates with F_v/F_m ($r = -0.976$; $p < 0.01$; Supplemental Figure 9D). One explanation for this correlation is that F_{min} may be disproportionately underestimated relative to F_{max} in shorter plants resulting in an artificially inflated F_v/F_m value. Although PlantCV is still a useful

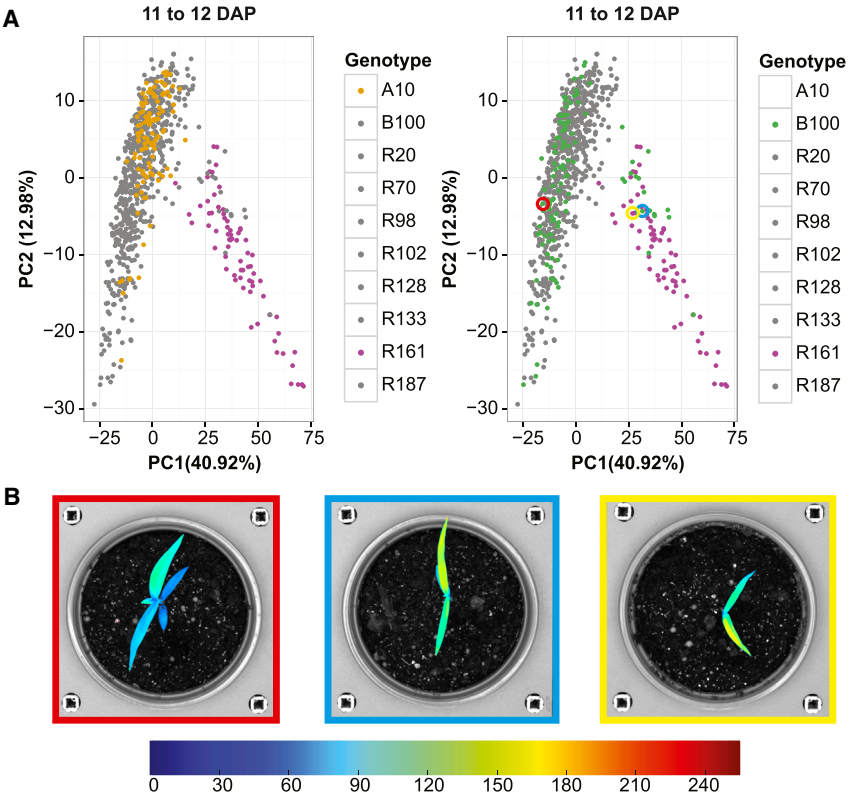

Figure 6. Before Water Treatment Is Applied (11–12 DAP) Color Can Distinguish *Setaria* Genotypes.

(A) PCA of RGB color for all *Setaria* genotypes before treatment is applied (11–12 DAP). PC1 and PC2 are plotted for *S. viridis* (orange), *S. italica* (green), RIL161 (purple), and seven other *S. viridis* × *S. italica* RILs (gray).

(B) *S. italica* (yellow circle in **(A)**; yellow boxed image) found among R161 (blue circle in **(A)**; blue boxed image) are more similar in color than *S. italica* (red circle in **(A)**; red boxed image) that group with other lines (gray). VIS images are pseudocolored based on the value channel in HSV color space. See also Supplemental Figures 5–8.

tool for analyzing photosynthetic efficiency, alterations in the physical configuration of the PSII imaging station are necessary to prevent height differences from confounding photosynthetic efficiency measurements.

NIR Image Processing and Traits

The NIR imaging station captures NIR light (900–1700 nm) using two cameras (320 × 256 pixel) mounted for top- and side-view imaging with a rotating lifter to allow for multiple side-view images. Four side-view (0°, 90°, 180°, and 270°) NIR images were captured per plant per time point. The NIR top-view camera was partially functioning during the experiment so top-view images were not taken at all time points. In addition, the background signal of soil in the top-view NIR images makes plant signal isolation difficult so only side-view NIR images were used in the analysis. In total, *Setaria* plants were imaged 6399 times from 11 to 33 DAP for a total of 25 596 NIR side-view images.

PlantCV isolation of plant material from other background components in NIR grayscale images is achieved through several image processing techniques, including background estimation/removal and object of interest sharpening to improve the effectiveness of binary thresholding. Once the plant is identified, the grayscale NIR pixel-level intensity is summarized into a histogram containing 256 bins, where each bin contains the proportion of plant pixels exhibiting the corresponding grayscale intensity value. Shape attributes described above for VIS imaging are also recorded for each NIR image for quality control purposes. Comparison of shape measurements between imaging stations allows for the detection of outliers due to artifacts in the image processing pipelines. Similarity of NIR signal within snapshot sets and image classes (genotype by treatment by DAP) using Chi-squared and Earth Mover's Distances were also used to assess data quality. For more information on NIR image processing please refer to the Supplemental Experimental Procedures.

NIR Signal Analysis

The effects of camera zoom level can be clearly observed as the camera imaging configuration changes from 3.1× to 1.4× optical zoom at 21 DAP (Figure 7A). Comparison of 100% and 33% FC water treatments as the mathematical difference of treatment-averaged histograms illustrates a shift in the distribution of NIR signal histogram toward increased NIR signal reflectance in drought-treated plants (Figure 7B).

PCA was used to summarize the changes observed in the NIR signal histograms. Due to the shifts in the NIR signal between zoom levels, PCA was done within each zoom level. While the first principal components (PC1s) at each zoom level are not directly comparable, the loadings indicate that they are driven by the same phenomenon; the two sides of the loading histograms with opposite signs indicate a shift from higher absorbance pixels, which have been associated with higher water content in previous studies, to lower absorbance pixels (Figure 7C and 7D) (Carter, 1991; Peñuelas and Filella, 1998; Seelig et al., 2008, 2009). PC1 captures a larger proportion of variation (33.5%) within NIR signals at the widest zoom level (1.4×), corresponding to later growth stages and more extended drought treatment, than PC1s from earlier narrower zoom levels (14.9% and 25.9% at 3.9× and 3.1×, respectively). Significant differences of PC1 values ($n = 8$; $p < 0.01$) compared between treatments (100% and 33% FC) were observed in both *S. viridis* and *S. italica* parental genotypes 23 DAP (Figure 8). The NIR system measures wavelengths of light that are absorbed by water but signal transmittance and reflectance can also change with differences in leaf thickness or tissue composition (Seelig et al., 2008, 2009; Neilson et al., 2015). Therefore, shifts in NIR signal due to differences in leaf water content cannot be distinguished from changes in leaf thickness or tissue composition in response to water deficit. More advanced imaging analysis, perhaps integrating VIS data, or additional

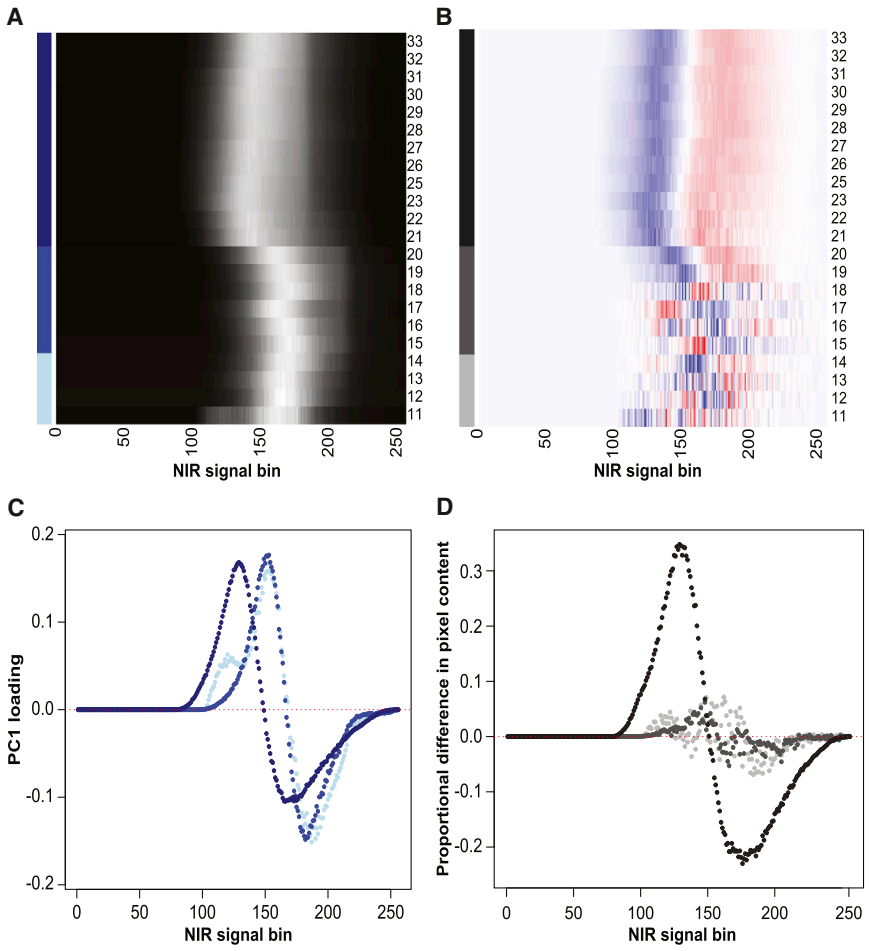

Figure 7. Measurements Derived from the NIR Camera System.

(A) Average NIR signal distribution of well-watered plants throughout the experiment. Bins corresponding to signal intensity levels 0–255 are plotted along the x-axis, while experimental days are plotted along the y-axis. The proportion of pixels that fall into each bin are expressed as a grayscale shade (0% black, larger percentages are increasingly more white). Color bars along the y-axis illustrate zoom range (3.9× = light blue, 3.1× = blue, 1.4× = dark blue).

(B) Difference of average NIR signal distribution between plants receiving 100% and 33% FC. Signal bins shaded blue have an increased proportion of pixels in images of plants receiving 100% FC water; signal bins shaded red have a greater proportion of pixels in images receiving 33% FC water; white corresponds to no difference between images.

(C) A plot of PC1 loadings (3.9× = light-gray, 3.1× = mid-gray, 1.4× = black).

(D) A plot of the average signal difference between water treatment levels 100% and 33% FC (3.9× = light-gray, 3.1× = mid-gray, 1.4× = black).

imaging hardware might be utilized to distinguish between these two water-deficit responses.

Integrated Analysis

While each extracted trait can be treated individually, multimodal traits can be used to detect artifacts or gain greater insight on biological responses. For example, correlations between plant height and F_v/F_m signal were used to identify the physical limitations of the PSII imaging station and examining biomass with watering data expanded understanding of WUE. Examining correlation between traits may identify simple biometric relationships inherent to a biological system (such as the positive correlation between plant biomass and height; Supplemental Figure 10) or more intricate relationships that are dependent on treatment or temporal factors (relationship between NIR PC1 and VIS color PC1 and PC2; Supplemental Figure 10). An important component of trait integration is an understanding of which traits are reporting precisely on genotype or treatment effects. On four days that span the experimental period, variance due to genotype, treatment, and genotype by treatment across the traits discussed was examined using a simple linear model (Table 1). Emphasizing the temporal dependence of the measured traits, there were notable shifts in which factor accounted for the largest components of variation at different time points. In the six days from 19 to 25 DAP, as the cumulative water deficit became more severe, the treatment term accounted for a much larger portion of the biomass, tiller count, and NIR PC1 variance, a trend that continues through 31 DAP. For WUE, treatment had the largest effect 19 DAP, reflecting the dynamic and differing response to water availability between *S. viridis* and *S. italica* (Figure 4). Temporal measurements allowed the identification of mechanistic differences in drought response, which would be indistinguishable with only end-point measurements.

Genotype accounted for at least 17.9% of the variance at one or more time point for all the traits described in Table 1, including PCA traits from color and NIR signal, suggesting that these traits will be tractable targets for temporal genetic and gene by environment analysis. Combined with the variance accounted for by treatment, it is clear that traits measured by the VIS and NIR systems can be used to investigate plant responses to a changing environment. An outstanding question is whether the distinct image types are contributing independent insights to an experiment. While analysis of eight RIL lines was sufficient to identify distinct responses in the two parents for multiple traits, it is not enough to determine if the traits are correlated or segregating independently from each other. Analysis of larger genetic populations is necessary to identify the underlying genetic loci for each trait and to determine if they segregate independently.

It is important to note that the analysis routines presented here are just a starting point for the data that can be extracted from the images collected. The most significant finding from the analysis is that wild *S. viridis* and domesticated *S. italica* have different responses to water availability. This result comes from analysis of

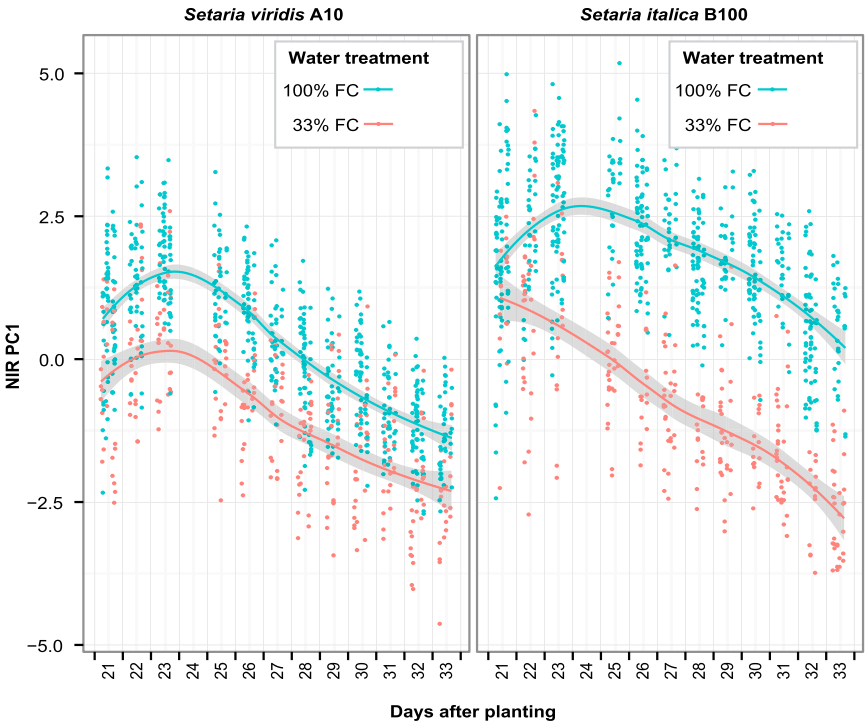

Figure 8. NIR PC1 Throughout Time While Zoom = 1.4× for *Setaria* genotypes *S. viridis* (A10) and *S. italica* (B100).
Plants watered to 100% or 33% FC are shown. Local regression (LOESS) fitted curves with SE are plotted for each genotype by water treatment group.

pixel-estimated biomass that does not require integration of plant architecture for accurate measure. However, integrating plant architecture by including identification of leaf and stem pixels as well as segmenting the plant by developmental age could extract further information from VIS and NIR images. Making the images and PlantCV software publically available is intended to encourage other researchers to join in on addressing these questions.

CONCLUSIONS

There are three essential components of the Bellwether Phenotyping Platform: tightly controlled and recorded environmental variables, automated image capture, and scriptable analysis by PlantCV. With all of the components in place, experiments can be conducted on a scale not previously possible. For example, without the four automatic watering stations in the growth chamber, maintaining the moisture level of 1140 pots in a high-light high-temperature environment would require considerable labor for the duration of the experiment. The design decisions that led to the high capacity of the platform permit repeated measurements of hundreds of lines with replicates and multiple treatments. Analysis by PlantCV allows for flexible and timely image processing and analysis. Open-source PlantCV software is platform independent, allowing it to scale from controlled-environment growth chamber phenotyping to field phenotyping. PlantCV is currently used to process images from four diverse custom-built imaging platforms at the Donald Danforth Plant Science Center. The image dataset provided by this study can be utilized to extend PlantCV function by extracting further architectural traits that are also important to crops with similar structure, such as maize and sorghum.

In this study, four different water regimes were imposed with multiple replicates for each line/treatment combination. Although only 10 *Setaria* lines were examined in the present study, this work showed that *S. viridis* and *S. italica* have fundamentally different responses to water availability. The wild accession *S. viridis* adjusts its growth to utilize all of the available water, while the domesticated *S. italica* is less efficient at converting water to biomass under high-water availability. Although the domesticated crop *S. italica* is known to be drought tolerant from previous studies (Li and Brutnell, 2011), differences between *S. viridis* and *S. italica* response to water availability would not have been detected if only end-point biomass or WUE were examined, highlighting the importance of temporal examination of traits. The eight randomly selected RILs displayed variation between the parents suggesting, unsurprisingly, that the observed traits are controlled by multiple loci. Therefore, future phenotyping studies using this system that examine a larger population of *S. viridis* × *S. italica* RILs will likely be successful in extracting multiple time-dependent drought-related quantitative trait loci.

MATERIALS AND METHODS

Plant Growth

Setaria Experiment Growth Details

White/gray pots (diameter 10 cm [4 inches]) from Hummert were pre-filled with ~473 ml of MetroMix360 soil and 0.5 g of Osmocote Classic 14-14-14 fertilizer (Everris, USA) was manually distributed to the top of each pot. *S. viridis* (A10), *S. italica* (B10), and eight RILs (RIL020, RIL070, RIL098, RIL102, RIL128, RIL133, RIL161, RIL187) from an *S. viridis* × *S. italica* population (Devos et al., 1998; Wang et al., 1998; Bennetzen et al., 2012) were planted, barcoded, then allowed to germinate for 9 days in a Conviron growth chamber before being loaded into the Conviron growth area of the Bellwether Phenotyping Platform. Barcoded information included genotype identification, water treatment group, and a unique pot identification number. During germination, plants were grown under a long-day photoperiod (16 h day/8 h night) at 31°C day/21°C night. During the germination period, the maximum light intensity of the Conviron chamber was used (230 μmol/m^2/s). At 9 DAP, germinated plants were loaded into the Conviron growth chamber of the Bellwether Phenotyping Platform using a random block design. In the phenotyping facility, plants were grown under a long-day photoperiod (16 h day/8 h night) at 31°C day/21°C night at a light intensity of 500 μmol/m^2/s using metal halide and high-pressure sodium lamps to deliver a broad spectrum of light for plant growth: 20.7% at 400–500 nm, 33.3% at 500–600 nm, 26.8% at 600–700 nm, 3.3% at 700–800 nm, and 15.8% at 800–900 nm (measured with Apogee Instruments Spectroradiometer PS-100).

Water Treatments

The 10-cm pre-filled pots were dried down to remove excess moisture from the soil. After dry down, the average dry pot, soil, and Osmocote weight was 73 g. To determine soil volume water content, measured

Variance type	Biomass	Height	Tiller count	WUE[a]	RGB.PC1[b]	RGB.PC2[c]	NIR.PC1[d]	DAP
Genotype	14.8	61.3	53.2	20.6	75.1	65.8	38.9	15
Treatment	0	0	0	0	0	0	0	
Genotype × treatment	5.2	2.4	0	5	0	1.8	2.5	
Residual	80	36.3	46.8	74.5	24.9	32.4	58.6	
Genotype	17.9	22.8	36.5	20.2	62.6	39.4	29.5	19
Treatment	4.8	0.4	2.8	27.8	0	0.3	6.7	
Genotype × treatment	7.2	5.3	5.2	4.4	0	1	5	
Residual	70.1	71.5	55.5	47.5	37.4	59.4	58.8	
Genotype	14.4	65.4	11.5	22.2	66.3	60.9	30.5	25
Treatment	55.4	1.8	66.9	8.2	13.9	0	56.7	
Genotype × treatment	4.6	4	6.7	5.6	0.9	7.3	4.1	
Residual	25.5	28.8	14.9	64	18.9	31.8	8.7	
Genotype	2.7	42.8	9.8	7.7	62.5	8.3	8.3	31
Treatment	83.7	7.3	78.9	8	7.7	1	75.5	
Genotype × treatment	2.1	8	1.9	0	5.6	13.9	3.8	
Residual	11.5	41.9	9.4	84.3	24.1	76.8	12.5	

Table 1. Proportion of Variance Explained by Experimental Factors.

Variance associated with factors genotype, experimental treatment, the interaction of genotype and treatment was assessed at four time points (15, 19, 25, 31 DAP). Unexplained variance is denoted as residual variance. See also Supplemental Figure 10.

[a]Water-use efficiency.

[b]The color (red, green, blue) first principal component.

[c]The color (red, green, blue) second principal component.

[d]The near-infrared first principal component.

amounts of reverse osmosis water were added to the dry soil and allowed to absorb for 1 h. Volume water content (VWC) was determined by a Decagon Devices GS3 soil moisture sensor and ProCheck Instantaneous data logger. The full-capacity water treatment group was assigned a target weight of 625 g. Given a carrier weight of 335 g and soil/pot dry weight of 73 g, the full-capacity treatment group corresponds to 217 ml of available water and a soil VWC of ~48%. Initially, five treatment group target weights were defined as 100%, 75%, 50%, 25%, and 0% of the soil/pot wet weight, which corresponded to the target weights 625 g, 552.5 g, 480 g, 407.5 g, and 0 g. However, accounting for only relative water availability, the treatments were 100% FC (217 ml; 48% VWC), 66.5% FC (144.5 ml; 31% VWC), 33% FC (72 ml; 14% VWC), and 0 ml for the remaining groups.

Hardware

The LemnaTec Scanalyzer 3D$^{H\text{-}T}$ is controlled using LemnaControl software. Image and water treatment data from the phenotyping facility are transferred to a PostgreSQL database (LemnaDB) for storage. PhenoFront (https://github.com/danforthcenter/PhenoFront) is used to access image data from the local LemnaTec database before image analysis with PlantCV (http://plantcv.danforthcenter.org/). For more information on the Conviron growth chamber specifications and camera specifications, please see the Supplemental Experimental Procedures.

PlantCV Image Processing and Data Capture

For a list of current measurements extracted by PlantCV, please refer to Supplemental Table 3. For more information on image processing pipelines, please refer to the Supplemental Experimental Procedures and for an example pipeline workflow, see Supplemental Figure 11. Images were processed using 10 CPU (Intel Xeon E7-8867L) on a Dell PowerEdge M910 blade server running CentOS 6.5. The code used for this manuscript was PlantCV release v1.0 and is available at GitHub (http://github.com/danforthcenter/plantcv) and archived at Figshare (http://dx.doi.org/10.6084/m9.figshare.1447311).

Statistical Analysis and Modeling

All statistical analyses were done in R (R Core Team, 2014). Additional packages used include analogue (Simpson, 2007), car (Fox and Weisberg, 2011), emdist (Urbanek and Rubner, 2012), ggplot2 (Wickham, 2009), grid (R Core Team, 2014), gridExtra (Auguie, 2012), lattice (Sarkar, 2008), lme4 (Bates et al., 2014), lubridate (Grolemund and Wickham, 2011), MASS (Venables and Ripley, 2002), mvtnorm (Genz and Bretz, 2009; Genz et al., 2014), nlme (Pinheiro et al., 2014), pls (Mevik et al., 2013), plyr (Wickham, 2011), qvalue (Dabney and Storey, 2015), rgl (Adler and Murdoch, 2014), scales (Wickham, 2014), and VennDiagram (Chen, 2014). R scripts for all analyses are provided in Supplemental Table 4. Detailed methods for the statistics and modeling throughout this article can be found in the Supplemental Experimental Procedures.

SUPPLEMENTAL INFORMATION

Supplemental Information is available at *Molecular Plant Online*.

FUNDING

This work was supported by the United States Department of Agriculture-National Institute of Food and Agriculture (MOW-2012-01361 to N.F. and 2014-67012-22269 to C.S.), National Science Foundation (MCB-1330562 to J.C.C., IIA-1355406 to T.C.M., IOS-1027542 to T.P.B, and IOS-1202682 to M.A.G.), United State Department of Energy (DOE-SC-008796 to T.P.B., T.C.M., and I.B. and DE-SC0006627 to T.C.M.), National Institutes of Health (AI043288 to J.C.C.) and United States Department of Agriculture Agricultural Research Service Intramural Funds (I.B.).

AUTHOR CONTRIBUTIONS

N.F., M.F., M.A.G., M.S.W., and I.B. conceptualized and collected the high-throughput phenotyping experiment. N.F., M.F., and M.A.G. designed and wrote the PlantCV image analysis software. D.W.B., S.T.H., and C.J.M. wrote the PhenoFront database access software. N.F., M.F., M.A.G., C.S., S.N.W., I.K., T.F., S.T., K.B.G., and I.B. conceptualized and executed trait validation experiments. N.F., M.F., M.A.G., C.S., and I.B. formally analyzed the data. N.F., M.F., M.A.G., M.S.W., C.S., and I.B. wrote the manuscript. T.P.B., J.C.C., T.C.M., and I.B., supervised and reviewed the manuscript.

ACKNOWLEDGMENTS

We would like to thank the Bellwether Foundation for the generous donation that allowed the construction of the Bellwether Phenotyping Platform, DDPSC Facilities for careful maintenance of the systems, Kevin Nagel for system training, Pu Huang and Dustin Mayfield-Jones for manual measurement assistance. No conflict of interest declared.

Received: May 5, 2015
Revised: May 28, 2015
Accepted: June 8, 2015
Published: June 20, 2015

REFERENCES

Abràmoff, M.D., Magalhães, P.J., and Ram, S.J. (2004). Image processing with ImageJ. Biophotonics Int. **11**:36–43.

Adler, D., and Murdoch, D. (2014). rgl: 3D Visualization Device System. R Package, version 0.93 1098.

Albrecht-Borth, V., Kauss, D., Fan, D., Hu, Y., Collinge, D., Marri, S., Liebers, M., Apel, K., Pfannschmidt, T., Chow, W.S., et al. (2013). A novel proteinase, SNOWY COTYLEDON4, is required for photosynthetic acclimation to higher light intensities in Arabidopsis. Plant Physiol. **163**:732–745.

Andrade-Sanchez, P., Gore, M.A., Heun, J.T., Thorp, K.R., Carmo-Silva, A.E., French, A.N., Salvucci, M.E., and White, J.W. (2014). Development and evaluation of a field-based high-throughput phenotyping platform. Funct. Plant Biol. **41**:68–79.

Auguie, B. (2012). gridExtra: Functions in Grid Graphics. R Package, version 0.91.

Bates, D., Mächler, M., Bolker, B., and Walker, S. (2014). Fitting Linear Mixed-Effects Models Using lme4. arXiv preprint, arXiv:1406.5823.

Benfey, P.N., and Mitchell-Olds, T. (2008). From genotype to phenotype: systems biology meets natural variation. Science **320**:495–497.

Bennetzen, J.L., Schmutz, J., Wang, H., Percifield, R., Hawkins, J., Pontaroli, A.C., Estep, M., Feng, L., Vaughn, J.N., Grimwood, J., et al. (2012). Reference genome sequence of the model plant *Setaria*. Nat. Biotechnol. **30**:555–561.

Berger, B., Parent, B., and Tester, M. (2010). High-throughput shoot imaging to study drought responses. J. Exp. Bot. **61**:3519–3528.

Bozdogan, H. (1987). Model selection and Akaike's Information Criterion (AIC): the general theory and its analytical extensions. Psychometrika **52**:345–370.

Bradski, G. (2000). The opencv library. Doctor Dobbs J. **25**:120–126.

Bray, E.A. (1997). Plant responses to water deficit. Trends Plant Sci. **2**:48–54.

Brutnell, T.P., Wang, L., Swartwood, K., Goldschmidt, A., Jackson, D., Zhu, X.-G., Kellogg, E., and Van Eck, J. (2010). *Setaria viridis*: a model for C4 photosynthesis. Plant Cell **22**:2537–2544.

Carter, G.A. (1991). Primary and secondary effects of water content on the spectral reflectance of leaves. Am. J. Bot. **78**:916.

Chen, H. (2014). VennDiagram: Generate High-Resolution Venn and Euler Plots. BMC Bioinformatics, 35.

Dabney, A., and Storey, J.D. (2015). qvalue: Q-Value Estimation for False Discovery Rate Control. R Package, version 1.26.0.

Darmency, H., Ouin, C., and Pernes, J. (1987). Breeding foxtail millet (*Setaria italica*) for quantitative traits after interspecific hybridization and polyploidization. Genome **29**:453–456.

Devos, K.M., Wang, Z.M., Beales, J., Sasaki, T., and Gale, M.D. (1998). Comparative genetic maps of foxtail millet (*Setaria italica*) and rice (*Oryza sativa*). Theor. Appl. Genet. **96**:63–68.

Doust, A.N. (2007a). Architectural evolution and its implications for domestication in grasses. Ann. Bot. **100**:941–950.

Doust, A.N. (2007b). Grass architecture: genetic and environmental control of branching. Curr. Opin. Plant Biol. **10**:21–25.

Doust, A.N., and Kellogg, E.A. (2006). Effect of genotype and environment on branching in weedy green millet (*Setaria viridis*) and domesticated foxtail millet (*Setaria italica*) (Poaceae). Mol. Ecol. **15**:1335–1349.

Doust, A.N., Kellogg, E.A., Devos, K.M., and Bennetzen, J.L. (2009). Foxtail millet: a sequence-driven grass model system. Plant Physiol. **149**:137–141.

Dudley, J.T., and Butte, A.J. (2009). A quick guide for developing effective bioinformatics programming skills. PLoS Comput. Biol. **5**:e1000589.

Fahlgren, N., Gehan, M.A., and Baxter, I. (2015). Lights, camera, action: high-throughput plant phenotyping is ready for a close-up. Curr. Opin. Plant Biol. **24**:93–99.

Fernández-García, N., Olmos, E., Bardisi, E., García-De la Garma, J., López-Berenguer, C., and Rubio-Asensio, J.S. (2014). Intrinsic water use efficiency controls the adaptation to high salinity in a semi-arid adapted plant, henna (*Lawsonia inermis* L.). J. Plant Physiol. **171**:64–75.

Fourment, M., and Gillings, M.R. (2008). A comparison of common programming languages used in bioinformatics. BMC Bioinformatics **9**:82.

Fox, J., and Weisberg, S. (2011). An R Companion to Applied Regression, 2nd edn (SAGE Publications).

Furbank, R.T., and Tester, M. (2011). Phenomics–technologies to relieve the phenotyping bottleneck. Trends Plant Sci. **16**:635–644.

Garg, A.K., Kim, J.-K., Owens, T.G., Ranwala, A.P., Choi, Y.D., Kochian, L.V., and Wu, R.J. (2002). Trehalose accumulation in rice plants confers high tolerance levels to different abiotic stresses. Proc. Natl. Acad. Sci. USA **99**:15898–15903.

Gentleman, R.C., Carey, V.J., Bates, D.M., Bolstad, B., Dettling, M., Dudoit, S., Ellis, B., Gautier, L., Ge, Y., Gentry, J., et al. (2004). Bioconductor: open software development for computational biology and bioinformatics. Genome Biol. **5**:R80.

Genz, A., and Bretz, F. (2009). In Computation of Multivariate Normal and t Probabilities, *Vol. 195* (Springer Science & Business Media).

Genz, A., Bretz, F., Miwa, T., Mi, X., Leisch, F., Scheipl, F., and Hothorn, T. (2014). mvtnorm: Multivariate Normal and t Distributions. R Package, version 0.9-2.

Gerland, P., Raftery, A.E., Sevcikova, H., Li, N., Gu, D., Spoorenberg, T., Alkema, L., Fosdick, B.K., Chunn, J., Lalic, N., et al. (2014). World population stabilization unlikely this century. Science **346**:234–237.

Gilbert, D. (2004). Bioinformatics software resources. Brief. Bioinform. **5**:300–304.

Goff, S.A., Vaughn, M., McKay, S., Lyons, E., Stapleton, A.E., Gessler, D., Matasci, N., Wang, L., Hanlon, M., Lenards, A., et al. (2011). The iPlant Collaborative: cyberinfrastructure for plant biology. Front. Plant Sci. **2**:34.

Golzarian, M.R., Frick, R.A., Rajendran, K., Berger, B., Roy, S., Tester, M., and Lun, D.S. (2011). Accurate inference of shoot biomass from high-throughput images of cereal plants. Plant Methods **7**:2.

Grolemund, G., and Wickham, H. (2011). Dates and times made easy with lubridate. J. Stat. Softw. **40**:1–25.

Hartmann, A., Czauderna, T., Hoffmann, R., Stein, N., and Schreiber, F. (2011). HTPheno: an image analysis pipeline for high-throughput plant phenotyping. BMC Bioinformatics **12**:148.

Honsdorf, N., March, T.J., Berger, B., Tester, M., and Pillen, K. (2014). High-throughput phenotyping to detect drought tolerance QTL in wild barley introgression lines. PLoS One **9**:e97047.

Hunter, J.D. (2007). Matplotlib: a 2D graphics environment. Comput. Sci. Eng. **9**:90–95.

IPCC. (2014). Climate change 2014: impacts, adaptation, and vulnerability. In Part A: Global and Sectoral Aspects. Contribution of Working Group II to the Fifth Assessment Report of the Intergovernmental Panel on Climate Change (Cambridge and New York, NY: Cambridge University Press).

Jia, G., Huang, X., Zhi, H., Zhao, Y., Zhao, Q., Li, W., Chai, Y., Yang, L., Liu, K., and Lu, H. (2013). A haplotype map of genomic variations and genome-wide association studies of agronomic traits in foxtail millet (*Setaria italica*). Nat. Genet. **45**:957–961.

Kellogg, E.A. (1999). Phylogenetic aspects of the evolution of C4 photosynthesis. In C4 Plant Biology, R.F. Sage and R.K. Monson, eds. (San Diego, CA: Academic Press), pp. 411–444.

Klukas, C., Chen, D., and Pape, J.-M. (2014). Integrated analysis platform: an open-source information system for high-throughput plant phenotyping. Plant Physiol. **165**:506–518.

Kremnev, D., and Strand, Å. (2014). Plastid encoded RNA polymerase activity and expression of photosynthesis genes required for embryo and seed development in *Arabidopsis*. Front. Plant Sci. **5**:385.

Kunz, H.-H., Gierth, M., Herdean, A., Satoh-Cruz, M., Kramer, D.M., Spetea, C., and Schroeder, J.I. (2014). Plastidial transporters KEA1, -2, and -3 are essential for chloroplast osmoregulation, integrity, and pH regulation in *Arabidopsis*. Proc. Natl. Acad. Sci. USA **111**:7480–7485.

Kvilekval, K., Fedorov, D., Obara, B., Singh, A., and Manjunath, B.S. (2010). Bisque: a platform for bioimage analysis and management. Bioinformatics **26**:544–552.

Lata, C., Sahu, P.P., and Prasad, M. (2010). Comparative transcriptome analysis of differentially expressed genes in foxtail millet (*Setaria italica* L.) during dehydration stress. Biochem. Biophys. Res. Commun. **393**:720–727.

Lata, C., Bhutty, S., Bahadur, R.P., Majee, M., and Prasad, M. (2011). Association of an SNP in a novel DREB2-like gene SiDREB2 with stress tolerance in foxtail millet (*Setaria italica* L.). J. Exp. Bot. **62**:3387–3401.

Li, P., and Brutnell, T.P. (2011). *Setaria viridis* and *Setaria italica*, model genetic systems for the Panicoid grasses. J. Exp. Bot. **62**:3031–3037.

Lobet, G., Draye, X., and Périlleux, C. (2013). An online database for plant image analysis software tools. Plant Methods **9**:38.

Mahfoozi, S. (2001). Developmental regulation of low-temperature tolerance in winter wheat. Ann. Bot. **87**:751–757.

Mangalam, H. (2002). The Bio* toolkits – a brief overview. Brief. Bioinform. **3**:296–302.

Maxwell, K., and Johnson, G.N. (2000). Chlorophyll fluorescence—a practical guide. J. Exp. Bot. **51**:659–668.

McCouch, S., Baute, G.J., Bradeen, J., Bramel, P., Bretting, P.K., Buckler, E., Burke, J.M., Charest, D., Cloutier, S., Cole, G., et al. (2013). Agriculture: feeding the future. Nature **499**:23–24.

Mevik, B.-H., Wehrens, R., and Liland, K.H. (2013). pls: Partial Least Squares and Principal Component Regression. R Package, version 2.

Munns, R., and Tester, M. (2008). Mechanisms of salinity tolerance. Annu. Rev. Plant Biol. **59**:651–681.

Neilson, E.H., Edwards, A.M., Blomstedt, C.K., Berger, B., Moller, B.L., and Gleadow, R.M. (2015). Utilization of a high-throughput shoot imaging system to examine the dynamic phenotypic responses of a C4 cereal crop plant to nitrogen and water deficiency over time. J. Exp. Bot. **66**:1817–1832.

Nelson, T., and Dengler, N. (1997). Leaf vascular pattern formation. Plant Cell **9**:1121–1135.

Oliphant, T.E. (2007). Python for scientific computing. Comput. Sci. Eng. **9**:10–20.

Paine, C.E.T., Marthews, T.R., Vogt, D.R., Purves, D., Rees, M., Hector, A., and Turnbull, L.A. (2012). How to fit nonlinear plant growth models and calculate growth rates: an update for ecologists. Methods Ecol. Evol. **3**:245–256.

Paproki, A., Sirault, X., Berry, S., Furbank, R., and Fripp, J. (2012). A novel mesh processing based technique for 3D plant analysis. BMC Plant Biol. **12**:63.

Peñuelas, J., and Filella, I. (1998). Visible and near-infrared reflectance techniques for diagnosing plant physiological status. Trends Plant Sci. **3**:151–156.

Phattaralerphong, J., and Sinoquet, H. (2005). A method for 3D reconstruction of tree crown volume from photographs: assessment with 3D-digitized plants. Tree Physiol. **25**:1229–1242.

Pinheiro, J., Bates, D., DebRoy, S., Sarkar, D., and Team, T.R.C. (2014). nlme: Linear and Nonlinear Mixed Effects Models. R Package, version 3.

Qie, L., Jia, G., Zhang, W., Schnable, J., Shang, Z., Li, W., Liu, B., Li, M., Chai, Y., and Zhi, H. (2014). Mapping of quantitative trait locus (QTLs) that contribute to germination and early seedling drought tolerance in the interspecific cross *Setaria italica*×*Setaria viridis*. PLoS One **9**:e101868.

Ray, D.K., Mueller, N.D., West, P.C., and Foley, J.A. (2013). Yield trends are insufficient to double global crop production by 2050. PLoS One **8**:e66428.

R Core Team. (2014). R: A Language and Environment for Statistical Computing.

Richards, R., and Thurling, N. (1978). Variation between and within species of rapeseed (*Brassica campestris* and *B. napus*) in response to drought stress. I. Sensitivity at different stages of development. Aust. J. Agric. Res. **29**:469.

Sage, R.F., and Zhu, X.-G. (2011). Exploiting the engine of C(4) photosynthesis. J. Exp. Bot. **62**:2989–3000.

Sarkar, D. (2008). Lattice: Multivariate Data Visualization with R. Springer Science & Business Media.

Satou, M., Enoki, H., Oikawa, A., Ohta, D., Saito, K., Hachiya, T., Sakakibara, H., Kusano, M., Fukushima, A., Saito, K., et al. (2014). Integrated analysis of transcriptome and metabolome of *Arabidopsis* albino or pale green mutants with disrupted nuclear-encoded chloroplast proteins. Plant Mol. Biol. **85**:411–428.

Schoffl, F. (1998). Regulation of the heat-shock response. Plant Physiol. **117**:1135–1141.

Seelig, H.-D., Hoehn, A., Stodieck, L.S., Klaus, D.M., Adams, W.W., III, and Emery, W.J. (2008). The assessment of leaf water content using leaf reflectance ratios in the visible, near-, and short-wave-infrared. Int. J. Remote Sens. **29**:3701–3713.

Seelig, H.-D., Hoehn, A., Stodieck, L.S., Klaus, D.M., Adams, W.W., and Emery, W.J. (2009). Plant water parameters and the remote sensing R 1300/R 1450 leaf water index: controlled condition

dynamics during the development of water deficit stress. Irrig. Sci. **27**:357–365.

Simpson, G.L. (2007). Analogue methods in palaeoecology: using the analogue package. J. Stat. Softw. **22**:1–29.

Talukder, S., Babar, M., Vijayalakshmi, K., Poland, J., Prasad, P., Bowden, R., and Fritz, A. (2014). Mapping QTL for the traits associated with heat tolerance in wheat (*Triticum aestivum* L.). BMC Genet. **15**:97.

Urbanek, S., and Rubner, Y. (2012). emdist: Earth Mover's Distance. R Package.

Venables, W.N., and Ripley, B.D. (2002). Modern Applied Statistics with S, 4th edn (New York: Springer).

Wang, Z.M., Devos, K.M., Liu, C.J., Wang, R.Q., and Gale, M.D. (1998). Construction of RFLP-based maps of foxtail millet, *Setaria italica* (L.) P. Beauv. Theor. Appl. Genet. **96**:31–36.

Warnasooriya, S.N., and Brutnell, T.P. (2014). Enhancing the productivity of grasses under high-density planting by engineering light responses: from model systems to feedstocks. J. Exp. Bot. **65**:2825–2834.

White, J.W., Andrade-Sanchez, P., Gore, M.A., Bronson, K.F., Coffelt, T.A., Conley, M.M., Feldmann, K.A., French, A.N., Heun, J.T., Hunsaker, D.J., et al. (2012). Field-based phenomics for plant genetics research. Field Crops Res. **133**:101–112.

Wickham, H. (2009). ggplot2: Elegant Graphics for Data Analysis. Springer Science & Business Media.

Wickham, H. (2011). The split-apply-combine strategy for data. J. Stat. Softw. **40**:1–29.

Wickham, H. (2014). scales: Scale Functions for Graphics. R package.

Wilkins, O., Bräutigam, K., and Campbell, M.M. (2010). Time of day shapes *Arabidopsis* drought transcriptomes. Plant J. **63**:715–727.

Zhang, J., Liu, T., Fu, J., Zhu, Y., Jia, J., Zheng, J., Zhao, Y., Zhang, Y., and Wang, G. (2007). Construction and application of EST library from *Setaria italica* in response to dehydration stress. Genomics **90**:121–131.